

Solution Branching and Dive Plane Reversal of Submarines at Low Speeds

Fotis A. Papoulias¹ and Jeffery S. Riedel²

The problem of multiple steady-state solutions in the dive plane of submarines under depth control at low speeds is analyzed. This phenomenon occurs regardless of the particular means used for depth control, manual or automatic, and linear or nonlinear. It is shown that the primary bifurcation parameter is a Froude-like number based on the vehicle speed and metacentric height. Generic solution branching is shown to occur below a critical Froude number. Singularity theory techniques are employed to quantify the effects that various vehicle geometric properties and hydrodynamic characteristics have on steady-state motion. It is demonstrated that a comprehensive bifurcation study provides a systematic and effective way of predicting the phenomenon of dive plane reversal at low speeds. A complete characterization of the parameters in the problem, both in deep water and at periscope depth, is achieved through the organizing center of the pitchfork singularity.

1. Introduction

ONE OF THE most critical functions of a submersible vehicle is accurate depth keeping at the commanded depth. Such a function can be carried out either manually or automatically, especially in cases where human intervention is impossible or undesirable. Due to the technological significance of the problem and the numerous scientific applications of submersible vehicle systems, design of appropriate depth keeping control laws has received wide attention. Such designs include linear and nonlinear controllers [Lindgren et al (1967)], [Gueler (1989)], model-based compensators [Healey (1992)], adaptive control [Goheen et al (1987)], and sliding mode control laws [Yoerger & Slotine (1985)], [Cristi et al (1991)]. Response accuracy and stability are the primary considerations in designing a depth keeping control law. Of paramount importance here are the robustness properties of the particular design; i.e., its ability to maintain accuracy and stability in the presence of incomplete sensor and environmental information, as well as actual/mathematical model mismatch. The scope of the work reported in this paper is to demonstrate a potential loss of stability that may occur when a submersible is operating at low speeds. This is a static loss of stability and should not be confused with the dynamic loss of stability that is usually associated with higher speeds. It is shown that such a loss of stability is accompanied by a slow divergence of trajectories away from the commanded path. Solution branching occurs in the form of generic pitchfork bifurcations [Golubitsky & Schaeffer (1985)]. A complete characterization of the problem is given utilizing singularity theory techniques, which have been proven very useful in the analysis of similar problems [Papoulias (1988, 1992)]. The use of bifurcation theory allows us to determine the crucial vehicle parameters that govern the problem of solution branching, and to develop guidelines to prevent its occurrence.

Finally, we present a new look at the problem of dive plane

reversal [Clayton & Bishop (1982)] based on solution branching results. The term "dive plane reversal" refers to a well-known phenomenon in submarine operations where during low-speed depth keeping there is a need for reversing the direction of dive plane deflection in order to execute a given change in depth. Physically, this can be explained by considering the relative magnitude of the hydrodynamic and hydrostatic forces. At moderate and high speeds, the normal force on the submarine's hull due to the angle of attack exceeds the normal dive plane force and the boat responds to ordered dive plane angles as expected. The phenomenon of dive plane reversal occurs at speeds below a certain critical speed in which the normal hull force is less than the normal dive plane force and the response of the boat is reversed. Vehicle modeling in this work follows standard notation [Gertler & Hagen (1967)] and numerical results are presented for the DARPA SUBOFF model [Roddy (1990)] for which a set of hydrodynamic coefficients and geometric properties is available. Special emphasis is given in identifying the proper nondimensional parameters in the problem, so that extension of the results to full-scale models and other designs is possible using a minimal set of experimental data and/or analytical results. Unless otherwise mentioned, all results are presented in standard nondimensional forms with the exception of angular deflections, which are shown in degrees.

2. Problem formulation

Equations of motion

Assuming that vehicle motion is restricted in the vertical plane, the mathematical model consists of the coupled nonlinear heave and pitch equations of motion. In a moving coordinate frame fixed at the vehicle's geometrical center, Newton's equations of motion for a port/starboard symmetric vehicle are expressed as follows:

$$\begin{aligned}
 m(\dot{w} - Uq - z_G q^2 - x_G \dot{q}) &= Z_q \dot{q} + Z_w \dot{w} \\
 &+ Z_q Uq + Z_w Uw - C_D \int_{\text{tail}}^{\text{nose}} b(x) \frac{(w - xq)^3}{|w - xq|} dx \\
 &+ (W - B) \cos \theta + U^2(Z_{\delta_s} \delta_s + Z_{\delta_b} \delta_b) \quad (1)
 \end{aligned}$$

¹Assistant professor, Naval Postgraduate School, Department of Mechanical Engineering, Monterey, California.

²Lieutenant, USN; Naval Postgraduate School, Department of Mechanical Engineering, Monterey, California.

Revised manuscript received at SNAME headquarters January 15, 1993.

$$I_y \dot{q} + m z_G w q - m x_G (\dot{w} - U q) = M_q \dot{q} + M_w \dot{w} + M_q U q + M_w U w - C_D \int_{\text{tail}}^{\text{nose}} b(x) \frac{(w - xq)^3}{|w - xq|} x dx - (x_G W - x_B B) \cos \theta - (z_G W - z_B B) \sin \theta + U^2 (M_{\delta_s} \delta_s + M_{\delta_b} \delta_b) \quad (2)$$

In equations (1) and (2), W is the vehicle weight, B the buoyancy, (x_G, z_G) the coordinates of the center of gravity, (x_B, z_B) the coordinates of the center of buoyancy, δ_s the stern plane angle, and δ_b the bow plane angle [Papoulias (1993)]. The cross flow integral terms in the above equations become important during hovering operations or low-speed maneuvering, whereas at high speeds U (and consequently low angles of attack with respect to the water) their effect is minimal. The drag coefficient, C_D , is assumed for simplicity to be constant throughout the vehicle length. This does not affect significantly the results that follow. The remaining symbols in (1) and (2) follow standard notation and are explained in the Nomenclature. We use U for the vehicle forward speed instead of the standard symbol u [Gertler & Hagen (1967)] in order to emphasize the fact that propulsion dynamics are assumed decoupled from the basic model and the forward speed remains constant in the equations of motion. All changes in the forward speed are assumed to be quasi-static, which is consistent with standard bifurcation theory assumptions.

The vehicle pitch rate is

$$\dot{\theta} = q \quad (3)$$

and the rate of change of depth

$$\dot{z} = -U \sin \theta + w \cos \theta \quad (4)$$

where θ is the pitch angle with respect to the nominal horizontal direction. The vehicle geometry and definitions for most of the above symbols are shown in Fig. 1. The forward velocity U is assumed to be kept constant by the propulsion control during depth keeping. Any changes in U are assumed to take place in a quasi-steady way, i.e., at a rate much slower than vehicle motions in the dive plane.

Control law

Equations (1) through (4) can be written as a set of four nonlinear coupled differential equations in the form

$$\dot{\theta} = q \quad (5)$$

$$\dot{w} = a_{11} U w + a_{12} U q + a_{13} z_{GB} \sin \theta + b_{11} U^2 \delta_s + b_{12} U^2 \delta_b + d_w(w, q) + c_1(w, q) \quad (6)$$

$$\dot{q} = a_{21} U w + a_{22} U q + a_{23} z_{GB} \sin \theta + b_{21} U^2 \delta_s + b_{22} U^2 \delta_b + d_q(w, q) + c_2(w, q) \quad (7)$$

$$\dot{z} = -U \sin \theta + w \cos \theta \quad (8)$$

where

$$D_v = (m - Z_w)(I_y - M_q) - (m x_G + Z_q)(m x_G + M_w)$$

$$a_{11} D_v = (I_y - M_q) Z_w + (m x_G + Z_q) M_w$$

$$a_{12} D_v = (I_y - M_q)(m + Z_q) + (m x_G + Z_q)(M_q - m x_G)$$

$$a_{13} D_v = -(m x_G + Z_q) W$$

$$b_{11} D_v = (I_y - M_q) Z_{\delta_s} + (m x_G + Z_q) M_{\delta_s}$$

$$b_{12} D_v = (I_y - M_q) Z_{\delta_b} + (m x_G + Z_q) M_{\delta_b}$$

$$a_{21} D_v = (m - Z_w) M_w + (m x_G + M_w) Z_w$$

$$a_{22} D_v = (m - Z_w)(M_q - m x_G) + (m x_G + M_w)(m + Z_q)$$

$$a_{23} D_v = -(m - Z_w) W$$

$$b_{21} D_v = (m - Z_w) M_{\delta_s} + (m x_G + M_w) Z_{\delta_s}$$

$$b_{22} D_v = (m - Z_w) M_{\delta_b} + (m x_G + M_w) Z_{\delta_b}$$

$$d_w(w, q) D_v = (I_y - M_q) I_w + (m x_G + Z_q) I_q$$

$$d_q(w, q) D_v = (m - Z_w) I_q + (m x_G + M_w) I_w$$

$$c_1(w, q) D_v = (I_y - M_q) m z_G q^2 - (m x_G + Z_q) m z_G w q$$

$$c_2(w, q) D_v = -(m - Z_w) m z_G w q + (m x_G + M_w) m z_G q^2$$

In equations (5) through (8), the vehicle is assumed to be neutrally buoyant ($W = B$), level ($x_G = x_B$), and statically stable ($z_G > z_B$). The terms I_w and I_q represent the cross flow

Nomenclature

\mathbf{a} = dummy independent variable	F_n = critical value of F_n	(x_B, z_B) = body-fixed coordinates of vehicle center of buoyancy
α = bow plane to stern plane deflection ratio	I = vehicle mass moment of inertia	(x_G, z_G) = body-fixed coordinates of vehicle center of gravity
$b(x)$ = local beam of the hull	$k, \frac{1}{k}, \frac{1}{k}, \frac{1}{k}$ controller gains in θ, w, q , and z , respectively	x_{GB} = center of gravity/center of buoyancy separation, $x_G - x_B$
β = nondimensional value of $\frac{x_{GB}}{-x_{GB} g / U^2}$	λ = Froude number, F_n squared	z = deviation off commanded depth
C_D = quadratic drag coefficient	m = vehicle mass	z_{GB} = vehicle metacentric height, $z_G - z_B$
γ = bifurcation unfolding parameter related to C_D	M = pitch moment	Z = heave force
δ_b = bow plane deflection	M_a = derivative of M with respect to a	Z_a = derivative of Z with respect to a
δ_s, δ = stern plane deflection	q = pitch rate	
F_n = Froude number based on vehicle speed and metacentric height	θ = vehicle pitch angle	
	U = vehicle forward speed	
	U_c = critical value of U	
	U_0 = nominal forward speed	
	w = heave velocity	

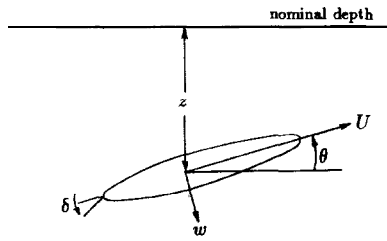


Fig. 1 Vehicle geometry and definitions of symbols

drag integrals in (1) and (2), and $z_{GB} = z_G - z_B$ is the metacentric height. Without loss in generality we can assume z_B to be zero, so that $z_{GB} = z_G$.

During most cruising operations, effective depth control can be achieved by using the linearized version of equations (5) through (8), where the linearization is performed around level flight path at the commanded depth. The linear system of equations that is then utilized for depth control law design is

$$\dot{\theta} = q \quad (9)$$

$$\dot{w} = a_{11}U_0w + a_{12}U_0q + a_{13}z_{GB}\theta + b_1U_0^2\delta \quad (10)$$

$$\dot{q} = a_{21}U_0w + a_{22}U_0q + a_{23}z_{GB}\theta + b_2U_0^2\delta \quad (11)$$

$$\dot{z} = -U_0\theta + w \quad (12)$$

where U_0 is the nominal speed for gain selection, a is defined as the bow plane to dive plane deflection ratio, and we have denoted

$$\begin{aligned} \delta_s &= \delta, \delta_b = \alpha\delta \\ b_1 &= b_{11} + \alpha b_{12}, \quad b_2 = b_{21} + \alpha b_{22} \end{aligned} \quad (13)$$

A linear full state feedback control law has the form [Friedland (1986)]

$$\delta = k_1\theta + k_2w + k_3q + k_4z \quad (14)$$

where the gains k_1, k_2, k_3, k_4 are computed such that the closed loop system (9) through (14) has the desired dynamics. If the desired characteristic equation has the general form,

$$\lambda^4 + \alpha_3\lambda^3 + \alpha_2\lambda^2 + \alpha_1\lambda + \alpha_0 = 0 \quad (15)$$

the controller gains can be computed by equating coefficients of the actual and desired characteristic equations,

$$b_1U_0^2k_2 + b_2U_0^2k_3 = -\alpha_3 - (a_{11} + a_{22})U_0 \quad (16)$$

$$\begin{aligned} b_2U_0^2k_1 + (b_2a_{12} - b_1a_{22})U_0^3k_2 + (b_1a_{21} - b_2a_{11})U_0^3k_3 \\ + b_1U_0^2k_4 = -\alpha_2 - a_{23}z_{GB} + (a_{11}a_{22} - a_{21}a_{12}) \end{aligned} \quad (17)$$

$$\begin{aligned} (b_2a_{11} - b_1a_{21})U_0^3k_1 + (b_1a_{23} - b_2a_{13})z_{GB}U_0^2k_2 \\ + (b_2 + b_1a_{22} - b_2a_{12})U_0^3k_4 \\ = \alpha_1 + (a_{13}a_{21} - a_{23}a_{11})z_{GB}U_0 \end{aligned} \quad (18)$$

$$[(b_1a_{21} - b_2a_{11})U_0^4 + (b_1a_{23} - b_2a_{13})z_{GB}U_0^3]k_4 = \alpha_0 \quad (19)$$

3. Solution branching

Numerical simulations

For demonstration purposes, assume that gain selection in (14) is based on a nominal speed $U_0 = 5$ ft/sec and a control time constant 3 dimensionless seconds. The control gains are computed from (16) through (19), while all initial conditions in the simulations are zero with the exception of depth, which is given an initial offset. The above set of nominal speed and

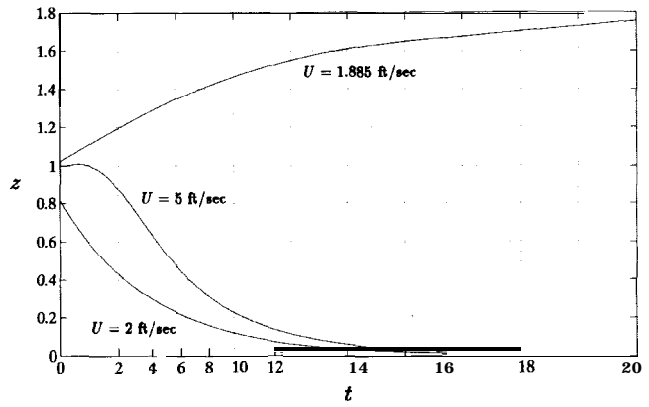


Fig. 2 Simulation results for different values of forward speed (time scale is $\times 100$ for $U = 1.885$ ft/sec, $\times 30$ for $U = 2$ ft/sec, and as is for $U = 5$ ft/sec)

gains selection generates a fast response and rejection of the initial disturbance as shown in Fig. 2, where we plot the dimensionless depth deviation (in vehicle lengths) versus dimensionless time (one unit is the time it takes to travel a vehicle length). When the vehicle speed is reduced, the response is more sluggish, as expected, due to the reduction of the forces and moments produced by the control surfaces. Nevertheless, convergence to the commanded value is still observed. Further reduction in the forward speed U , however, results in marginal convergence or even divergence away from the commanded level flight path, as Fig. 2 demonstrates. It appears from extensive simulation results that below a certain critical speed, U_c , the vehicle stabilizes to a nonzero steady state off the commanded set point. Preliminary studies of the problem in this section are conducted through steady-state, eigenvalue, and controllability analyses.

Steady-state solutions

Since we maintain the assumption $x_G = x_B$, it is expected that at steady state the heave velocity w will be small and, consequently, the cross flow integral drag terms I_w, I_q can be neglected. Steady state solutions are computed from $\theta = \dot{w} = \dot{q} = \dot{z} = 0$, and using equations (5) through (8) we get

$$q = 0$$

$$a_{11}Uw + a_{13}z_{GB} \sin \theta + b_1U^2\delta = 0$$

$$a_{21}Uw + a_{23}z_{GB} \sin \theta + b_2U^2\delta = 0$$

$$w \cos \theta - U \sin \theta = 0$$

or

$$w = U \tan \theta$$

$$\delta = \frac{(a_{13}a_{21} - a_{23}a_{11})z_{GB}}{(b_2a_{11} - b_1a_{21})U^2} \sin \theta \quad (20)$$

where θ is a solution to

$$(a_{11}b_2 - a_{21}b_1)U^2 \tan \theta + (a_{13}b_2 - a_{23}b_1)z_{GB} \sin \theta = 0 \quad (21)$$

Equation (21) admits the trivial solution $\theta = 0$ always, which results in $w = \delta = z = 0$, i.e., level steady-state motion at

the commanded depth. Besides $\theta = 0$, (21) may produce two more symmetric solutions in θ given by

$$\cos \theta = \frac{(a_{11}b_2 - a_{21}b_1)U^2}{(a_{23}b_1 - a_{13}b_2)z_{GB}} \quad (22)$$

Equation (22) is meaningful if $|\cos \theta| \leq 1$, which yields

$$U^2 \leq \frac{a_{23}b_1 - a_{13}b_2}{a_{11}b_2 - a_{21}b_1} z_{GB} \quad (23)$$

Substituting the expressions for a_{ij}, b_i in (23) we can find the critical value of the forward speed

$$U_c^2 = \frac{Z_\delta W}{M_w Z_\delta - Z_w M_\delta} z_{GB} \quad (24)$$

where we have denoted

$$Z_\delta = Z_{\delta_s} + \alpha Z_{\delta_b}, \quad M_\delta = M_{\delta_s} + \alpha M_{\delta_b}$$

For values of $U \leq U_c$, three steady-state solutions exist, the trivial solution at the commanded path and two solutions symmetrically located with respect to the trivial solution. Substituting the values $\alpha = 0, z_{GB} = 0.1$ ft in (24), we find $U_c = 1.898$ ft/sec, which is in agreement with the simulation results of Fig. 2.

A zero eigenvalue

The closed-loop linearized system at any forward speed U is given by

$$\dot{\theta} = q$$

$$\dot{w} = (a_{11}U + b_1U^2k_2)w + (a_{12}U + b_1U^2k_3)q + (a_{13}z_{GB} + b_1U^2k_1)\theta + b_1U^2k_4z$$

$$\dot{q} = (a_{21}U + b_2U^2k_2)w + (a_{22}U + b_2U^2k_3)q + (a_{23}z_{GB} + b_2U^2k_1)\theta + b_2U^2k_4z$$

$$\dot{z} = -U\theta + w$$

with characteristic equation of the form

$$A\lambda^4 + B\lambda^3 + C\lambda^2 + D\lambda + E = 0 \quad (25)$$

Comparing equation (25) and equations (16) through (19), we can see that the coefficient E is given by

$$E = [(b_1a_{21} - b_2a_{11})U^4 + (b_1a_{23} - b_2a_{13})z_{GB}U^2]k_4 \quad (26)$$

A real eigenvalue of (25) crosses zero when $E = 0$, which yields the same critical value U_c as (24). This is a typical pitchfork bifurcation which generically occurs in certain dynamical systems when a real eigenvalue of the linearized system crosses zero [Guckenheimer & Holmes (1983)]. At the pitchfork bifurcation point, the trivial equilibrium solution becomes unstable and two symmetric equilibrium positions appear. These pitchfork bifurcations are classified as supercritical if the two symmetric solutions appear after the trivial solution loses its stability, and in such a case they are asymptotically stable. In case that the opposite is true and that the new solutions are unstable and coexist with the stable trivial equilibrium solution, the pitchfork is said to be subcritical [Stewart & Thompson (1986)]. Although our numerical integrations suggest that the pitchfork bifurcations in this problem are supercritical, a detailed investigation of this along with practical implications and asymmetry effects is undertaken in Section 4.

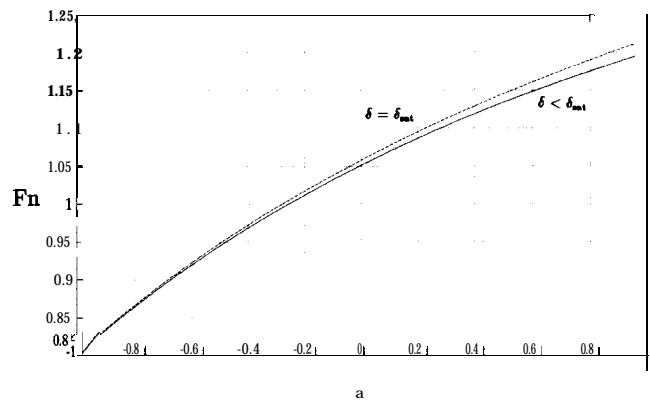


Fig. 3 Critical Froude number versus bow to dive plane deflection ratio

Results and discussion

Equation (24) suggests that the critical parameter that governs loss of stability and solution branching is a Froude-like number based on the metacentric height

$$Fn = \frac{U}{\sqrt{gz_{GB}}} \quad (27)$$

The critical Froude number is then

$$Fn_c = \left[\frac{Z_\delta W}{(M_w Z_\delta - Z_w M_\delta)g} \right]^{1/2} \quad (28)$$

Although the use of the term "Froude" number for a fully submerged body may seem questionable, it should be borne in mind that the current problem is totally different than flow prediction or resistance calculations. The concept of a Froude number signifies a relationship between hydrodynamic and hydrostatic forces, and that is exactly what equation (28) reflects. In fact, it is natural to expect that a Froude number based on the metacentric height will govern dive plane reversal since the phenomenon occurs as a certain balance between inertial (angle of attack) and gravitational (metacentric restoring) moments is achieved. A plot of the critical Froude number, Fn_c , versus the bow plane to dive plane deflection ratio, α , is shown in Fig. 3. The nonzero solutions in θ are computed from (22), the steady-state dive plane angle from (20), and the depth deviation from the control law (14). These computations are valid if the value of δ is less than its saturation limit δ_{sat} , which is typically set at ± 0.4 radians. In case where the computed δ exceeds δ_{sat} , the nonzero equilibrium pitch angle cannot be determined from (22). This means that $\dot{z} \neq 0$ at steady state, and the simplest condition is then $\dot{z} = \text{const}$. [Papoulias (1993)]. This allows for a semi-equilibrium state in which $\dot{z} = \theta = \dot{q} = \dot{w} = 0$. The steady-state solutions can then be computed from

$$a_{11}Uw + a_{13}z_{GB} \sin \theta + b_1U^2\delta_{sat} = 0$$

$$a_{21}Uw + a_{23}z_{GB} \sin \theta + b_2U^2\delta_{sat} = 0$$

or

$$\sin \theta = \frac{(b_2a_{11} - b_1a_{21})U^2\delta_{sat}}{(a_{13}a_{21} - a_{23}a_{11})z_{GB}} \quad (29)$$

A plot of the steady state value of θ versus Fn is shown in Fig. 4, where it can be seen that the saturation limit δ_{sat} is quickly reached. The critical Froude number for which $\delta = \delta_{sat}$ is shown by the dotted curve in Fig. 3. The fact that

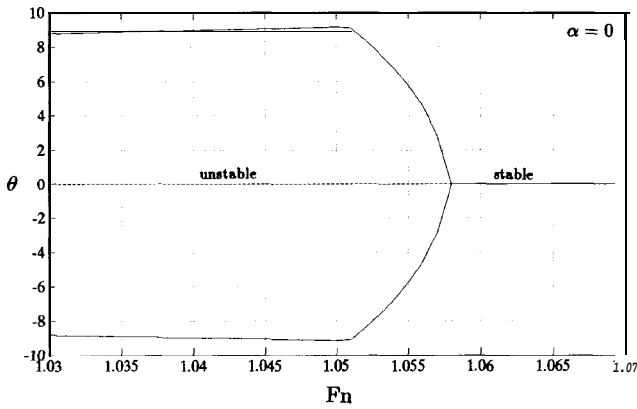


Fig. 4 Steady-state pitch angle versus Froude number

these values are located very close to F_n , means that the steady-state values of θ will appear locally in the vicinity of U_c as almost vertical in U . This result is directly related to the problem of dive plane reversal as discussed in Section 5.

Controllability

The controllability matrix [Friedland (1986)] of the linear, time invariant, single-input system

$$\dot{x} = Ax + b\delta \quad (30)$$

is the square matrix

$$\mathcal{C} = [b, Ab, A^2b, A^3b] \quad (31)$$

As long as \mathcal{C} is a nonsingular matrix, system (30) is state controllable, which means that an arbitrary change in the state vector x in finite time is possible through the use of a certain amount of control effort δ . In our case we have

$$A = \begin{bmatrix} 0 & 0 & 1 & 0 \\ a_{13}z_{GB} & a_{11}U & a_{12}U & 0 \\ a_{23}z_{GB} & a_{21}U & a_{22}U & 0 \\ -U & 1 & 0 & 0 \end{bmatrix}, \quad b = \begin{bmatrix} 0 \\ b_1U^2 \\ b_2U^2 \\ 0 \end{bmatrix} \quad (32)$$

A plot of the determinant of \mathcal{C} versus F_n for $\alpha = 0$ is shown in Fig. 5, where it can be seen that the critical speed could also have been defined as the speed at which the closed-loop system (30) becomes uncontrollable. Therefore, we can sum-

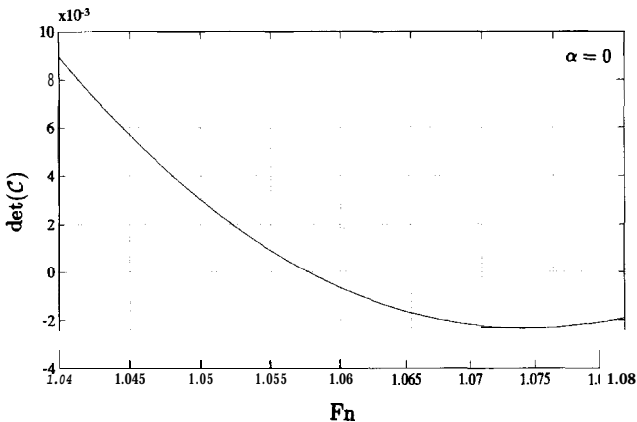


Fig. 5 Determinant of controllability matrix versus F_n for $\alpha = 0$

marize our findings by stating that there exists a vehicle critical speed for which (i) the straight-line level flight path becomes unstable, (ii) additional nonzero symmetric stable equilibrium positions appear, and (iii) the closed-loop depth control system is uncontrollable.

4. Pitchfork bifurcations

Pitchfork recognition

In the general case, steady-state solutions are computed from equations (1) through (4). A straight forward algebraic reduction process results in a single equation in w :

$$(Z_w M_\delta - M_w Z_\delta)Uw - C_D A_w (M_\delta - x_A Z_\delta)w|w| + [(W - B)M_\delta + (x_G W - x_B B)Z_\delta] \cos \theta + Z_\delta (z_G W - z_B B) \sin \theta = 0 \quad (33)$$

where,

$$\sin \theta = \frac{w}{\sqrt{w^2 + U^2}}, \quad \cos \theta = \frac{U}{\sqrt{w^2 + U^2}}$$

$$A_w = \int b(x) \& \\ x_A = \frac{1}{A_w} \int xb(x) dx$$

It is clear that equation (33) may admit multiple solutions in w . The remaining state variables are uniquely determined from w as

$$q = 0,$$

$$\theta = \tan^{-1} \left(\frac{w}{U} \right)$$

$$\delta = \frac{1}{U^2 Z_\delta} [C_D A_w w|w| - Z_w U w - (W - B) \cos \theta]$$

$$z = \frac{1}{k_4} (\delta - k_1 \theta - k_2 w)$$

The most interesting case in applications is for a neutrally buoyant vehicle, $W = B$. The case $W - B \neq 0$ is examined in Section 5. With the assumption $W = B$, equation (33) becomes

$$(Z_w M_\delta - M_w Z_\delta)Uw - C_D A_w (M_\delta - x_A Z_\delta)w|w| + x_{GB} B Z_\delta \frac{U}{\sqrt{U^2 + w^2}} + Z_\delta z_{GB} B \frac{w}{\sqrt{U^2 + w^2}} = 0 \quad (34)$$

where z_{GB} is the metacentric height and $x_{GB} = x_G - x_B$ the LCG/LCB separation.

Our goal is to analyze (34), which we refer to in compact form as

$$G(w, U, z_{GB}, x_{GB}) = 0$$

in terms of the pitchfork singularity

$$f(w, \lambda) = w^2 + \lambda w$$

In particular, we need to show that there exists a unique point $(w_c, U_c, x_{GB,c})$ which belongs to a set of physically accepted parameter values such that the primary bifurcation problem $G(w, U, x_{GB}) = 0$ is equivalent to the pitchfork $w^3 + \lambda w = 0$ in a neighborhood of (w_c, U_c) . According to bifurcation theory [Golubitsky & Schaeffer (1979) we must show

that there exists a unique solution to the system of equations

$$G = G_w = G_U = G_{ww} = 0 \quad (35)$$

in the three unknowns w, U, x_{GB} . The main difficulty in solving (35) directly lies in the fact that the dependence on w of the derivatives is highly nonlinear. We deal with this difficulty as follows.

We use Taylor series expansions to $\mathcal{O}(w^4)$ order

$$\frac{U}{\sqrt{U^2 + w^2}} \approx \frac{2U^2 - w^2}{2U^2}, \quad \frac{w}{\sqrt{U^2 + w^2}} \approx \frac{2wU^2 - w^3}{2U^3}$$

and we write (34) in the form

$$w^3 + \gamma\lambda w|w| - 2U^2(1 + \zeta\lambda)w + 2\beta U^2\lambda + \beta\lambda w^2 + 0 \quad (36)$$

where we have introduced the parameters

$$\lambda = \frac{U^2}{g z_{GB}}$$

$$\beta = -\frac{x_{GB} g}{U^2}$$

$$\gamma = 2UC_D A_w (M_\delta - x_A Z_\delta) \frac{g}{Z_\delta B}$$

$$\zeta = \frac{g(Z_w M_\delta - M_w Z_\delta)}{Z_\delta B}$$

The primary bifurcation parameter, A , remains the same as before, i.e., a Froude number squared based on the meta-centric height. The remaining three unfolding parameters have their origins in distinct physical properties. Parameter β represents another Froude-like number based on the LCG/LCB separation and is related to the vessel's trim and ballast conditions. Parameter γ is directly proportional to the quadratic drag coefficient C_D , while ζ summarizes the effects of the vehicle/planes linear hydrodynamics. One of the main motivations for using bifurcation theory is the ability to reduce the effect of all physical parameters to a small set of four coefficients, namely A, β, γ , and ζ .

The symmetric case, $x_{GB} = 0$ or $\beta = 0$, results in

$$w^3 + \gamma\lambda w|w| - 2U^2(1 + \zeta\lambda)w = 0 \quad (37)$$

or $g(w, A) = 0$. Obviously, $w = 0$ is a solution of $g(w, A) = 0$ for all A . This solution loses its stability at a critical value λ_c such that

$$1 + \zeta\lambda_c = 0 \text{ or } A_c = -\frac{1}{\zeta}$$

which, using the definitions for ζ, A , produces the same critical Froude number as (28). For values of A below A_c , equation (37) admits two nonzero solutions in w .

For nonzero values of β , a simplified pitchfork can be obtained from (36) by neglecting the higher-order terms $\lambda w|w|, \lambda w^2$:

$$w^3 - 2U^2(1 + \zeta\lambda)w + 2\beta U^2\lambda = 0 \quad (38)$$

or

$$h(w, A, \beta) = 0$$

To find the critical (A, β) curve we have to solve the system

$$h(w, A, \beta) = h_w(w, A, \beta) = 0 \quad (39)$$

Writing out (39) and eliminating w , we obtain

$$27\beta^2\lambda^2 = 8U^2(1 + \zeta\lambda)^3 \quad (40)$$

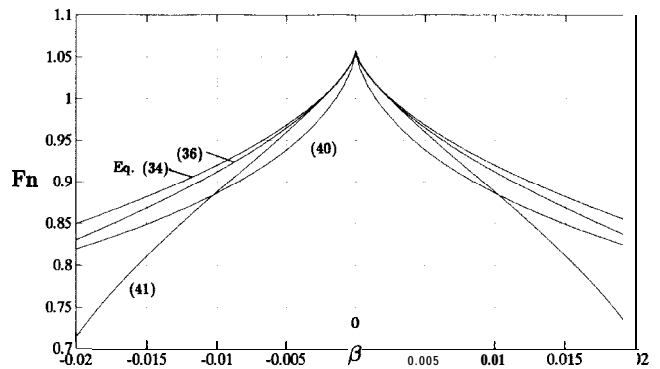


Fig. 6 Cusp comparisons for $C_D = 0$

An approximate solution of (40) can be found by rewriting it as $\beta^2 = f(\lambda)$ and expanding in Taylor series in A in the vicinity of the critical value $A_c = -1/\zeta$ for $\beta = 0$. This procedure yields

$$\lambda = -\frac{1}{\zeta} + \frac{3}{2} \left(\frac{\beta^2}{U^2 \zeta^4} \right)^{1/3} \quad (41)$$

Equation (41) provides an approximation to the critical (A, β) curve for small values of β and for A located close to its symmetric critical value $-1/\zeta$. It can be seen that this curve takes the form of a symmetric cusp with its origin located at $\beta = 0$. For values of the parameters (A, β) inside the cusp curve, equation (38) admits three solutions in w , one of which is unstable and two stable. By suitable smooth variable changes, (38) can be written as

$$w^3 + A'w + \beta' = 0 \quad (42)$$

which is recognized as a subtle pitchfork bifurcation [Stewart & Thompson (1986)]. This completes the recognition problem.

Bifurcation sets

A comparison of the previous cusp curves is shown in Fig. 6 in the $(\sqrt{\lambda}, \beta)$ parameter space and for $\gamma = 0$ (or $C_D = 0$). The use of $\sqrt{\lambda} \equiv Fn$ is employed so that direct comparison with the results of Section 3 is possible. The four cusp curves of Fig. 6 correspond to the bifurcation sets of the exact equation (34), its pitchfork approximation (36), the simplified pitchfork (40), and its analytic approximation (41). It can be seen that all four curves exhibit similar qualitative features in the vicinity of $\beta = 0$, namely the existence of a symmetric cusp located at $\beta = 0$. For higher values of β , the above approximations are no longer accurate and only the exact cusp curves should be utilized. The exact cusp curves for different values of the quadratic drag coefficient C_D are compared in Fig. 7. It can be seen that the effect of increasing C_D is to decrease the critical Froude number for a given value of β .

For a given nonzero value of β (or x_{GB}), the exact solution set $(0, Fn)$ is computed from equation (34) using $w = U \tan \theta$. Typical results are presented by the solid curves of Fig. 8 for $C_D = 0$, $z_{GB} = 0.1$ ft, and $x_{GB} = 0.01\%L$. Comparing Fig. 8, with Fig. 4, which was obtained for $x_{GB} = 0$, we can see that the previous pitchfork bifurcation is highly nonpersistent. Slight nonzero variations in x_{GB} , one hundredth of 1% of the vehicle length in this case, destroy the degenerate graph of Fig. 4 in favor of the asymmetry observed in Fig. 8. The original pitchfork point becomes now a turning point at a

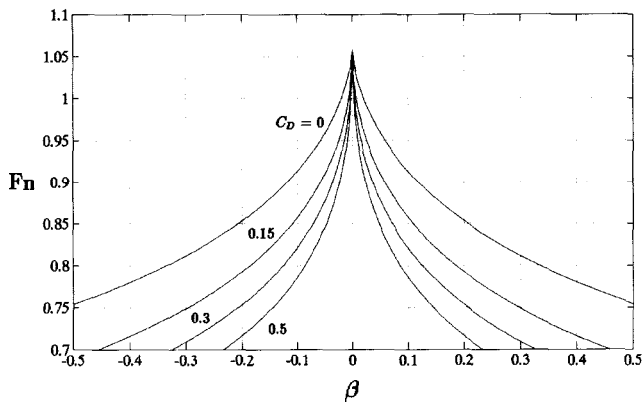


Fig. 7 Exact cusp curves for different values of C_D

critical Froude number considerably smaller than the critical value for $x_{GB} = 0$. The stability properties of the steady-state solutions remain the same as before; that is, for values of F_n below its critical value the two outer solutions are stable while the innermost solution is unstable. This biased pitchfork bifurcation is frequently called a saddle-node bifurcation [Guckenheimer & Holmes (1983)] since at the critical point a stable equilibrium (a node) coalesces with an unstable equilibrium (a saddle), resulting in their mutual destruction.

Since control surface saturation is not included in (34), the steady-state solutions in θ are allowed to reach unrealistically high values. In the case where $\delta = \delta_{sat}$, we have $w \neq U \tan \theta$, and steady-state values of w , θ can be computed from

$$Z_w U w - C_D A_w w |w| + Z_\delta U^2 \delta_{sat} = 0 \quad (43)$$

$$M_w U w - C_D x_A A_w w |w| - x_{GB} B \cos \theta - z_{GB} B \sin \theta + M_\delta U^2 \delta_{sat} = 0 \quad (44)$$

where we use $\delta_{sat} = \pm 0.4$ radians. These solutions are presented in Fig. 8 by the dashed curves, where it can be seen that the main result of control surface saturation is to significantly limit the steady state pitch angle. Unlike the symmetric case studied in Section 3, the Froude number at which control surface saturation occurs is not necessarily less than the critical Froude number at the turning point. This

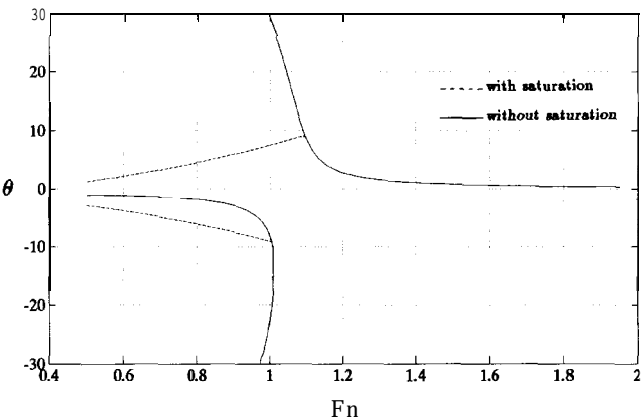


Fig. 9 Solution set (θ, F_n) for $x_{GB} = 0.01L$ and $C_D = 0$

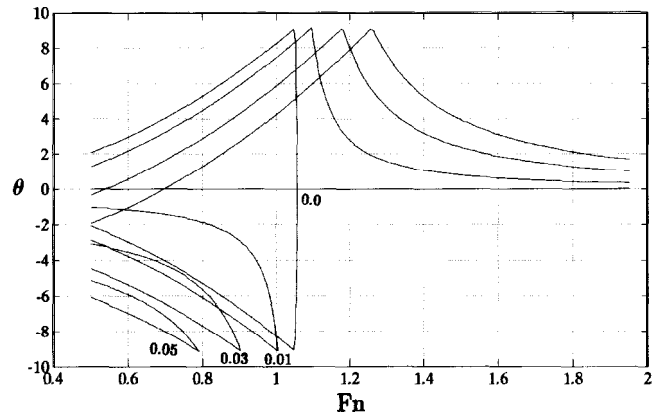


Fig. 9 Solution sets (θ, F_n) for different values of x_{GB} in %L and $C_D = 0$

is further demonstrated by the solution sets of Fig. 9 which are computed for $C_D = 0$, different values of x_{GB} , and include saturation effects. The effect of quadratic drag related terms, $C_D \neq 0$, is examined later in this section. Figure 9 suggests that the critical Froude number where multiple solutions appear may be different when saturation occurs. In order to modify the previous cusp curves by including saturation effects, we proceed as follows. We eliminate w from (43) and (44) and we get, with $C_D = 0$

$$x_{GB} B Z_w \cos \theta + z_{GB} B Z_w \sin \theta + (Z_\delta M_w - M_\delta Z_w) U^2 \delta_{sat} = 0 \quad (45)$$

If control surface saturation does not occur, the steady-state value for θ is computed from

$$x_{GB} B Z_\delta \cos \theta + z_{GB} B Z_\delta \sin \theta + (Z_w M_\delta - M_w Z_\delta) U^2 \tan \theta = 0 \quad (46)$$

Elimination of θ from (45) and (46) produces the critical (U, x_{GB}) curve for a given value of δ_{sat} . The elimination process produces an equation of the form

$$x_{GB} B Z_w - z_{GB} B Z_\delta \delta_{sat} + (Z_\delta M_w - M_\delta Z_w) U^2 \delta_{sat} \left[1 + \left(\frac{Z_\delta \delta_{sat}}{Z_w} \right)^2 \right]^{1/2} = 0 \quad (47)$$

in terms of the physical variables (U, x_{GB}) , or

$$\zeta \delta_{sat} \frac{\sqrt{Z_w^2 + Z_\delta^2 \delta_{sat}^2}}{Z_\delta B} = -\beta \frac{Z_w}{Z_\delta} - \frac{\delta_{sat}}{\lambda} \quad (48)$$

in terms of the bifurcation parameters (λ, β) . The saturation cusp curve (47) is plotted in Fig. 10 (solid curve) along with the exact bifurcation cusp curve (dashed curve) in the (F_n, x_{GB}) parameter plane. The number of steady-state solutions of our system can be obtained from these cusp curves in the following way:

- . Region A: one stable solution in θ with $\delta < \delta_{sat}$.
- . Region B: one stable solution in θ with $\delta = \delta_{sat}$.
- . Region C: three solutions in θ , two stable and one unstable, and $\delta < \delta_{sat}$ for all.
- . Region D: three solutions in θ , $\delta = \delta_{sat}$ for the two stable solutions, and $\delta < \delta_{sat}$ for the third unstable solution.

The case of $C_D \neq 0$ can be analyzed similarly. The saturation cusp curve can be computed from (43) and (44) with $w = U \tan \theta$. In this case, analytic reduction is not possible

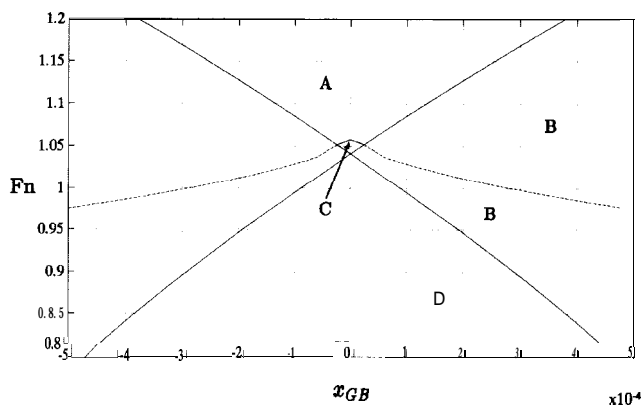


Fig. 10 Cusp curves in the (x_{GB}, Fn) parameter space, including saturation effects, with $C_D = 0$

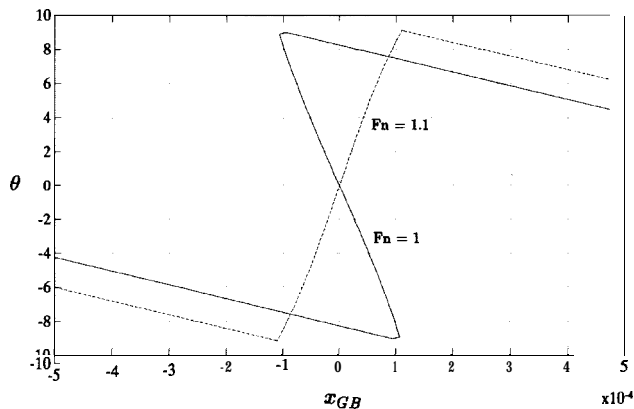


Fig. 12 Hysteresis unfolding for two paths through the cusp

any more. Instead, equation (43) is first solved for θ , and then equation (44) produces the critical value for x_{GB} . Typical results are presented in Fig. 11 for different values of the quadratic drag coefficient C_D . Since regions A and B are not associated with a change in the number of steady-state solutions, they do not appear explicitly in the figure. Furthermore, it can be seen that in reality it is the saturation cusp that dominates the character of the solution set, and in the following figures it is the only curve that is presented in the graphs.

Cusp catastrophe and path formulation

The cusp curve depicted in Fig. 10 can be utilized to predict the solution set for any physically realizable path in the (x_{GB}, Fn) parameter space. The cusp catastrophe is a term extensively used in singularity theory where it represents the universal unfolding of the curve x^3 and is given by $x^3 - Bx + A = 0$. A projection of this surface onto the unfolding space, i.e., the (A, B) -plane, produces the cusp curve $27A^2 = 4B^3$. This curve separates those (A, B) regions where $x^3 - Bx + A = 0$ has three or one real solutions in x . Although in our case the steady-state solutions are characterized by an equation considerably more complicated than $x^3 - Bx + A = 0$, it has been shown that the corresponding parameter regions in the (x_{GB}, Fn) space are separated by a similar cusp curve. We have already seen the corresponding solution sets for variations in the forward speed while keeping x_{GB} con-

stant. Of practical importance are "horizontal" paths through the cusp as well, i.e., keeping speed constant and changing the loading condition, x_{GB} . Consider two such paths where x_{GB} is varied between $\pm 0.03\%L$ and for two different speeds corresponding to Froude numbers $Fn = 1.1$ and $Fn = 1.0$. In the first case the path is located outside of the cusp, and the solution set, presented in terms of θ in Fig. 12, remains a single valued function for all values of x_{GB} . Smoothness of the solution set is destroyed when the outer saturation curves are crossed but this is not associated with any kind of bifurcation phenomena. The second path, corresponding to $Fn = 1.0$, cuts through the cusp and exhibits a typical hysteresis curve. Between the two extreme values of x_{GB} of the inner saturation curve of Fig. 10, the solution set is a triple-valued function in x_{GB} . The two outer solutions are asymptotically stable while the inner is unstable. This may give rise to sudden jump phenomena in the response as the weight distribution of the boat is slowly varying. Solution sets for more complicated paths, obtained by varying both speed, U , and ballast conditions, x_{GB} , as well as $C_D \neq 0$, can also be easily predicted by drawing the appropriate curve and observing its intersections with the cusp.

5. Dive plane reversal

A brief description of the need for dive plane reversal was given in the Introduction in terms of the relative magnitudes of control surface and hull-generated hydrodynamic forces. The phenomenon is usually described in terms of the neutral angles as well. This is a plot of the pitch angle and stern plane deflection required for straight and level flight versus the ship speed, and for a given loading condition, x_{GB} . At high speeds these neutral angles remain essentially constant. Both the pitch angle, θ , and the dive plane angle, δ_s , have the same sign and they can generate enough lift to counter the hydrostatic imbalance moment. As the speed is decreased, it becomes increasingly difficult to maintain the pitch angle on the hull and counteract the metacentric moment. Below the critical speed both θ and δ_s must reverse sign to maintain neutral trim. The results that were obtained through the use of bifurcation theory in this work formalized the above qualitative conclusions and identified the important nondimensional parameters that govern dive plane reversal.

Another way of viewing the problem is through the term k_4 in the control law (14). This represents a certain measure of the normal force that is required in order to respond to a unit change in depth. In terms of the forward speed U_o , this

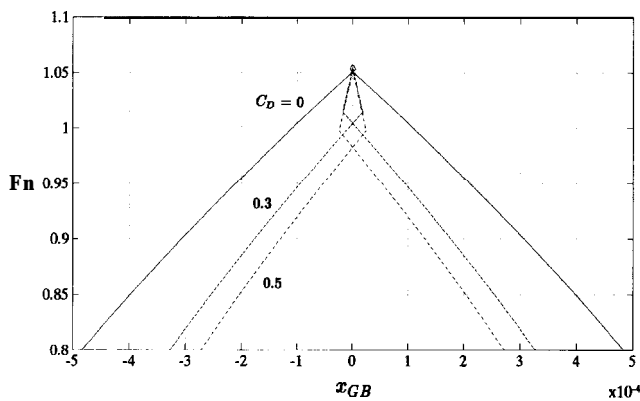


Fig. 11 Cusp curves in the (x_{GB}, Fn) parameter space for different values of C_D

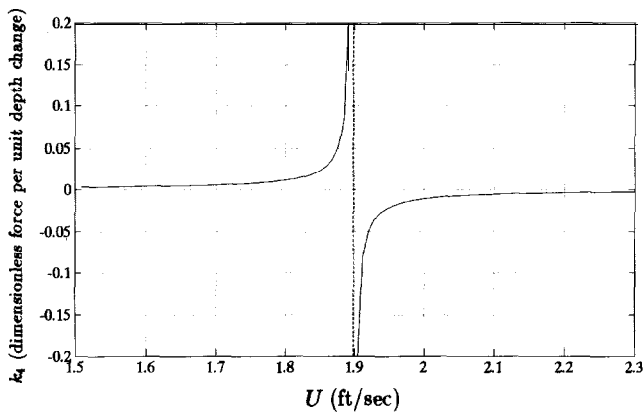


Fig. 13 Normal control force required per unit change in depth

term can be directly computed from equation (19). The corresponding plot is shown in Fig. 13 in dimensionless values. It can be seen from both Fig. 13 and equation (19), that k_4 approaches infinity at the critical speed U_c . This agrees with our previous conclusions that the systems is uncontrollable at that precise speed. Furthermore, the sign of k_4 is reversed as the critical speed is crossed, which results in the need for dive plane reversal in order to execute the same ordered depth change.

The case $W - B \neq 0$ can be studied using the same general approach. The most interesting case here is excess buoyancy, i.e., $W - B > 0$. This models, in a simplified way, a system bias that appears in free-surface suction effects. In such a case the solution set must be computed from equation (33). In view of the results of the previous section, however, it can be concluded that the cusp produced by (33) is of limited practical value. Instead, we need to consider the saturation cusp curve. This is produced by the generalization of equations (43) and (44):

$$Z_w U w - C_D A_w w |w| + (W - B) \cos \theta + U^2 Z_\delta \delta = 0 \quad (49)$$

$$M_w U w - C_D x_A A_w w |w| - (x_G W - x_B B) \cos \theta - (z_G W - z_B B) \sin \theta + U^2 M_\delta \delta = 0 \quad (50)$$

where we allow for $W \neq B$. Since we are computing the saturation cusp we can substitute $w = U \tan \theta$ and $\delta = \delta_{\text{sat}}$ in these equations. Then (49) can be solved numerically for θ , and (50) can be used to generate the critical curve. Typical results are presented in Figs. 14, and 15 for different values of the quadratic drag coefficient C_D and excess buoyancy $B - W$. The dramatic effect that a small value of nonzero bias force has is evident by studying these curves. The curves are significantly distorted and multiple intersections with a vertical path through the cusp with varying vehicle forward speed are possible. This signals transitions from one steady state to three, then to one, and then back to three in a manner that is typically associated with the winged cusp singularity [Golubitsky & Schaeffer (198511). These patterns are, of course, very sensitive to the ballast condition or the bias heave force and pitch moment.

So far we have concentrated on dive plane reversal, since it is more usual in operations. A fairwater plane reversal can also occur as well, typically at speeds higher than dive plane reversal. This phenomenon can be studied using the previously developed techniques; the analysis is virtually identical. Since we have parameterized the bow plane to stern plane deflection by a single parameter, α , dive plane usage corresponds to $\alpha = 0$ while bow plane usage to $\alpha \rightarrow \infty$. There-

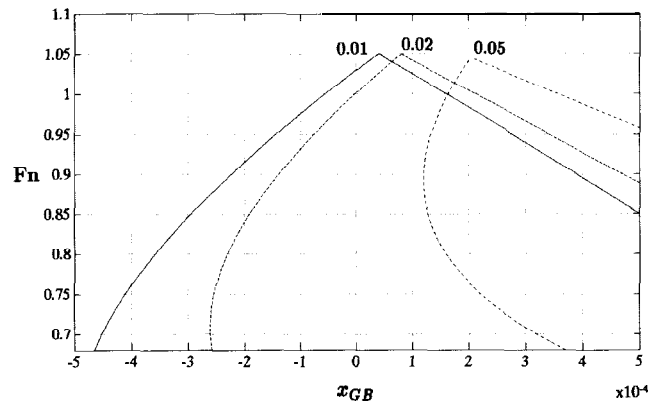


Fig. 14 Saturation cusp curves for $C_D = 0$ and different values of excess buoyancy $B - W$ in % W

fore, if we consider the critical speed in the limit $\alpha \rightarrow \infty$, we should produce the result for fairwater plane reversal. Alternatively, we could redefine α as the ratio of stern to bow plane deflection. Then $\alpha = 0$ would correspond to fairwater plane usage and the previous analysis would carry through in exactly the same way [Riedel (1993)]. This is demonstrated by the results of Fig. 16 where it can be seen that

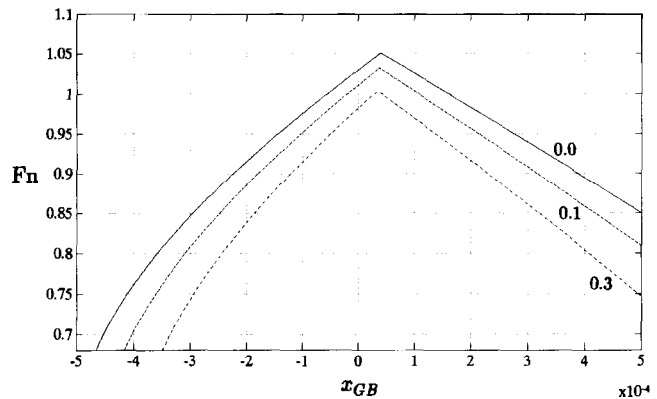


Fig. 15 Saturation cusp curves for $B - W = 0.01\%W$ and different values of C_D

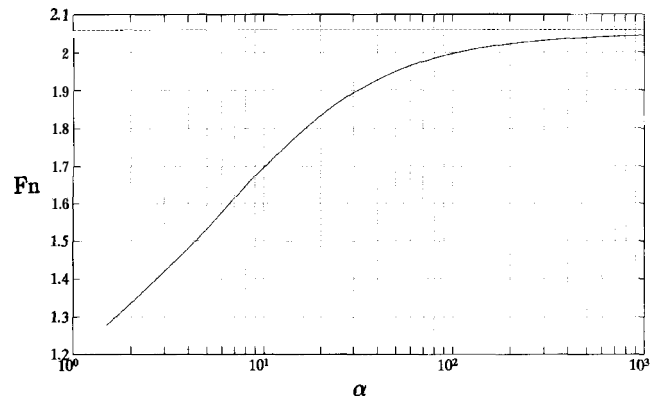


Fig. 16 Fairwater plane reversal: limiting value of critical speed

by allowing $\alpha \rightarrow \infty$ we approach the critical speed that corresponds to fairwater plane reversal.

6. Concluding remarks

A comprehensive study of multiple steady-state solutions in the vertical plane and submarine dive plane reversal has been presented. The analysis demonstrated the occurrence of supercritical pitchfork bifurcations for speeds below a critical value. Complete classification of the solution sets for different system parameters was achieved through the cusp. Numerical computations established the global validity of the singularity theory results. The main conclusions of this work can be summarized as follows:

- There exists a critical vehicle speed at which one real eigenvalue of the closed-loop depth-keeping linearized system matrix crosses zero. The nominal equilibrium state becomes unstable in a divergent way for speeds less than critical.

- Below the critical speed, two symmetric stable equilibrium positions appear. These are characterized by nonzero pitch angle and depth. They persist for a very limited speed-range since at such low speeds, control surface deflections reach their saturation limits quickly. Further reductions in the forward speed result in divergent motion with constant steady-state pitch angle and rate of change of depth.

- The closed-loop depth control system becomes uncontrollable at precisely the critical speed. The depth deviation error gain approaches infinity at that speed and it changes its sign. This means that as the critical speed is crossed, the direction of deflection of dive planes must be changed in order to maintain similar depth-changing response.

- The use of bifurcation theory facilitated the identification of three basic parameters that govern response. The primary bifurcation parameter is a Froude-like number based on vehicle speed and metacentric height. The primary unfolding parameter is also a Froude-like number based on vehicle speed and the longitudinal center of buoyancy/center of gravity separation. As secondary unfolding parameters we used the quadratic drag coefficient and the amount of excess buoyancy. The latter can be thought of as modeling the effects of heave bias, typically associated with near-surface operations.

- Construction of cusp curves in the primary two-dimensional parameter plane allowed the identification of solution sets for a number of different parameter variations. Pitchfork and hysteresis solution sets were shown to occur depending on the particular parameter path through the cusp.

- The two Froude-like numbers that were identified should be used in order to transition experimental results from

models to full scale. Unlike flow force prediction, the problem of dive plane reversal of a fully submerged body follows appropriate Froude scaling.

Acknowledgments

The authors would like to recognize the financial support of the Naval Postgraduate School Direct Research Fund.

References

- CLAYTON, B. R. AND BISHOP, R. E. D. 1982 *Mechanics of Marine Vehicles*. Gulf Publishing Company, Houston.
- CRISTI, R. PAPOULIAS, F. A. AND HEALEY, A. J. 1991 Adaptive sliding mode control of autonomous underwater vehicles in the dive plane. *IEEE Journal of Oceanic Engineering*, 15, 3.
- FRIEDLAND, B. 1986 *Control System Design: An Introduction to State-Space Methods*. McGraw-Hill, New York.
- GERTLER, M. AND HAGEN, G. R. 1967 Standard equations of motion for submarine simulation. David Taylor Research Center Report 2510, Bethesda, Md.
- GOEEN, K. R., JEFFERYS, E. R. AND BROOME, D. R. 1987 Robust self-designing controllers for underwater vehicles. *Journal of Offshore Mechanics and Arctic Engineering, Trans. ASME*, 109, 170–178.
- GOLUBITSKY, M. AND SCHAEFFER, D. 1979 A theory for imperfect bifurcation via singularity theory. *Communications on Pure and Applied Mathematics*, 32, 21–98.
- GOLUBITSKY, M. AND SCHAEFFER, D. G. 1985 *Singularities and Groups in Bifurcation Theory I*. Applied Mathematical Sciences 51, Springer-Verlag, New York.
- GUCKENHEIMER, J. AND HOLMES P. 1983 *Nonlinear Oscillations, Dynamical Systems, and Bifurcations of Vector Fields*. Applied Mathematical Sciences 42, Springer-Verlag, New York.
- GUELER, G. F. 1989 Modelling, design and analysis of an autopilot for submarine vehicles. *International Shipbuilding Progress*, 36, 405.
- HEALEY, A. J. 1992 Model-based maneuvering controls for autonomous underwater vehicles. *Journal of Dynamic Systems, Measurements, and Control, Trans. ASME*, 114, 614–622.
- LINDGREN, A. G., CRETELLA, D. B., AND BESSACINI, A. F. 1967 Dynamics and control of submerged vehicles. *Trans., Instrument Society of America*, 6, 4.
- PAPOULIAS, F. A. 1988 A qualitative and quantitative study of steady state response of towed floating bodies, *Dynamics and Stability of Systems*, 3, 3 & 4.
- PAPOULIAS, F. A. 1992 Stability and bifurcations of towed underwater vehicles in the dive plane. *JOURNAL OF SHIP RESEARCH*, 36, 3, Sept.
- PAPOULIAS, F. A. 1993 Dynamics and bifurcations of pursuit guidance for vehicle path keeping in the dive plane. *JOURNAL OF SHIP RESEARCH*, 37, 2, June.
- RIEDEL, J. S. 1993 Pitchfork bifurcations and dive plane reversal of submarines at low speeds. Mechanical Engineer's Thesis, Department of Mechanical Engineering, Naval Postgraduate School, Monterey, Calif.
- RODDY, R. F. 1990 Investigation of the stability and control characteristics of several configurations of the DARPA SUBOFF model (DTRC model 5470) from captive-model experiments. David Taylor Research Center Report DTRC/SHD-1298-08, Bethesda, Md.
- STEWART, H. B. AND THOMPSON, J. M. T. 1986 Towards a classification of generic bifurcations in dissipative dynamical systems. *Dynamics and Stability of Systems*, 1, 1.
- YOERGER, D. R. AND SLOTINE, J.-J. E. 1985 Robust trajectory control of underwater vehicles. *IEEE Journal of Oceanic Engineering*, 10, 4.